Cell. Mol. Life Sci. 62 (2005) 2877–2885
1420-682X/05/232877-9
DOI 10.1007/s00018-005-5322-x

Cellular and Molecular Life Sciences

Research Article

Functionally independent subunits in the oligomeric structure of the GABA cotransporter rGAT1

A. Soragna*, E. Bossi, S. Giovannardi, R. Pisani and A. Peres

Laboratory of Cellular and Molecular Physiology, Department of Structural and Functional Biology, and Center for Neurosciences, University of Insubria, Via Dunant 3, 21100 Varese (Italy), Fax: +39 0332 421300, e-mail: andrea.soragna@uninsubria.it

Received 18 July 2005; received after revision 21 September 2005; accepted 6 October 2005
Online First 28 November 2005

Abstract. We have combined structural and functional approaches to investigate the role of oligomerization in the operation of the GABA transporter rGAT1. *Xenopus laevis* oocytes were induced to express, either separately or simultaneously, the wild-type form of rGAT1 and a mutated (Y140W) form, unable to translocate GABA and to generate transport currents, although its intramembrane charge movement properties are only slightly affected. These characteristics, together with the insensitivity of Y140W to the blocking action of SKF89976A, were used to study the possible functional interaction of the two forms in an heteromeric structure. The electrophysiological data from oocytes coexpressing wild-type and Y140W rGAT1 were consistent with a completely independent activity of the two forms. Oligomerization was also studied by fluorescence resonance energy transfer (FRET) in tsA201 cells expressing the transporters fused with cyan and yellow fluorescent proteins (ECFP and EYFP). All combinations tested (WT-ECFP/WT-EYFP, Y140W-ECFP/Y140W-EYFP and WT-ECFP/Y140W-EYFP) were able to give rise to FRET, confirming the formation of homo- as well as heterooligomers. We conclude that, although rGAT1 undergoes structural oligomerization, each monomer operates independently.

Key words. Cotransporter; GABA; oligomerization; FRET; Xenopus oocytes.

Introduction

Oligomerization appears to be a common feature in the quaternary structure of neurotransmitter transporters. Its occurrence has in fact been demonstrated, using different approaches, in transporters belonging to different genetic families. Glutamate transporters, for example, have been shown to form homomultimers [1], and in particular, to be assembled in a trimeric complex which has been conserved during the evolution from prokaryotes to humans [2]. This kind of quaternary structure has been confirmed in the recently published crystallographic structure of a bacterial homologue of glutamate transporters [3]. In the past years, a freeze fracture analysis, based on the proportionality of the cross-sectional area of the particles and the number of membrane-spanning α-helices, was performed on the glutamate transporter EAAT3 overexpressed in Xenopus oocytes [4]. Based on an estimated number of 35 ± 2 α-helices, these authors postulated a pentameric assembly; however, considering the described peculiar topology of glutamate transporters [5], this number of helices is still compatible with a trimeric structure. Strong indications about the formation of oligomers were also found for the Na^+/Cl^--dependent neurotransmitter transporters (reviewed in [6]), that share the ability to couple the reuptake of the substrate to the sodium gradient across the plasma membrane [7]. These

* Corresponding author.

proteins also have a common topological model consisting in 12 putative membrane-spanning segments, with cytosolic C- and N-terminal domains. This secondary structure has been confirmed by the recently published crystal structure of $LeuT_{Aa}$, a bacterial homologue of the Na^+/Cl^--dependent neurotransmitter transporters [8], also showing an oligomeric quaternary structure as previously described in almost all the transporters of this family, with the only exception of glycine transporters 1 and 2, which were shown to exist as monomers at least in the plasma membrane [9]. Biochemical evidence indicated the existence of oligomeric complexes in the norepinephrine (NET) [10], serotonin (SERT) [11, 12] and dopamine (DAT) transporters [13]. This latter has been investigated in more detail using a cross-linking assay [14–16]: DAT has been shown to form dimers of dimers with two symmetrical interfaces in transmembrane domains 4 and 6. Besides the biochemical experiments, another interesting approach used to study oligomerization is FRET (Fluorescence Resonance Energy Transfer) between subunits tagged with fluorescent molecules. FRET is a quantum physical phenomenon based on non-radiative transfer of energy between two fluorescent molecules in close proximity (<100 Å) and in an appropriate relative orientation. Using variants of the green fluorescent protein (GFP) fused to the proteins of interest, FRET has already be shown to be valuable in the study of trimeric G proteins [17], in the dimerization of β-adrenergic receptors [18] and in the conformational rearrangements of ion channels [19]. The FRET methodology has also been applied to neurotransmitter transporters, revealing the close proximity and the possible formation of oligomeric structures in DAT [20] and in SERT [21]; also the γ-aminobutyric acid (GABA) transporter subtype 1 (GAT1) has been shown to generate FRET [21]. Similarly to the case of DAT, experiments aimed to understand how these complexes are formed indicated two additional interfaces believed important for the assembly of the multimeric protein: transmembrane domain 2 of GAT1, with a leucine heptad repeat and polar interactions [22, 23], and an interaction region in transmembrane domains 11 and 12 of SERT [24]. Although all these experimental data strongly suggest that Na^+/Cl^- dependent neurotransmitter transporters exist in multimeric complexes, generally formed by four identical subunits, the impact of this structure on the functionality of these proteins remains elusive. No clear evidence either for or against a functional role for oligomerization have been found yet. The formation of oligomeric complexes appears to be important for the correct targeting of the transporters to the membrane, although additional functional roles could not be excluded. In fact, experimental evidence indicates a functional interaction between the subunits of hSERT dimers [12], and the functional oligomerization of hNET and hDAT [13, 25]. Furthermore, a very interesting countertransport model for monoamine transporters has recently been proposed [26]. On the other hand, in vesicles prepared from HEK293 cells expressing a GAT1 mutant which abolishes oligomerization and leads to intracellular retention of the protein, a wild-type-like activity, in terms of GABA affinity and turnover number of uptake, has been observed [22], indicating that the functional unit might be the monomer. In this regard a FRET-based approach looking at conformational changes associated with glutamate uptake by EAAT3 suggests that, although associated in trimers, subunits function independently [27]. Furthermore, in a recently published paper Grewer and co-workers [28], using electrophysiological and biochemical approaches, demonstrated the subunit independence of glutamate transporter homotrimer.

In this scenario we used electrophysiological and FRET approaches in order to identify the functional unit of the rat GAT1 (rGAT1), taking advantage of a mutation (Y140W, [29]) which has peculiar electrophysiological features. This mutant is correctly inserted in the plasma membrane, and is still able to interact with external sodium ions giving rise to voltage-dependent transient currents; but its ability to transport GABA and to interact with the specific rGAT1 blocker SKF89976A is completely lost. These characteristics make Y140W ideal for investigating oligomerization-related negative dominance effects in coinjection experiments with wild-type GAT1.

Materials and methods

Construction of rGAT1-EYFP and rGAT1-ECFP and rGAT1 mutant Y140W

To obtain constructs useful for FRET experiments, rGAT1 from pAMV (generous gift of C. LaBarca) was subcloned in pECFP-N1 and pEYFP-N1 (Clontech, BD Bioscience, Milan, Italy) between *Sac*I and *Pst*I; this last restriction site was inserted by point mutation on the stop codon in frame with the ATG site of ECFP and EYFP, that result then fused in the COOH terminus of rGAT1.

Mutation Y140W of rGAT1 in all constructs (rGAT1-pECFP-N1, rGAT1-pEYFP-N1 and rGAT1-pAMV) was obtained by site-directed mutagenesis (Quickchange Site-Directed Mutagenesis Kit, Stratagene Inc., Mmedical, Milan, Italy).

All constructs were verified by sequencing (MWG Biotech, Sequencing Service, Ebersberg, Germany). For oocyte injection, complementary RNAs (cRNAs) encoding the wild-type and the Y140W mutant transporters were in vitro synthesized from *Not*I-linearized rGAT1-pAMV in the presence of Cap Analog and 200 units of T7 RNA polymerase. All enzymes were supplied by Promega Italia (Milan, Italy).

Xenopus laevis oocyte expression

Xenopus laevis frogs were anaesthetized in MS222 (tricaine methansulfonate) 0.10% (w/v) solution in tap water, and portions of ovary were removed through a small incision on the abdomen. The frogs were humanely killed after the collection. The oocytes were treated with collagenase (Sigma Type IA) 1 mg/ml in ND96 Ca^{2+} free solution (ND96 solution: NaCl 96 mM, KCl 2 mM, $MgCl_2$ 1 mM, $CaCl_2$ 1.8 mM, HEPES 5 mM, pH 7.6), for at least 1 h at 18 °C. Healthy-looking stage V and VI oocytes were collected and injected with 12.5 ng of total cRNA in 50 nl of water, using a manual microinjection system (Drummond). Oocytes were maintained in NDE solution (ND96 solution supplemented with 2.5 mM sodium pyruvate and 50 μg/ml gentamicin) and were tested 3–5 days after injection. The experiments were carried out according to the institutional and national ethical guidelines.

Electrophysiology and data analysis

Classic two-electrode voltage clamp (GeneClamp, Axon Instruments Foster City, CA, USA or Oocyte Clamp OC-725B, Warner Instruments, Hamden, CT, USA) was used to record membrane currents under voltage-controlled conditions. Reference electrodes were connected to the experimental oocyte chamber via agar bridges (3% agar in 3 M KCl) to minimize chloride effects on junction potential. Borosilicate electrodes, with a tip resistance of 0.5–2 MΩ, were filled with 3 M KCl. The holding potential (V_h) was kept at –40 mV, except when stated otherwise; voltage pulses to test potentials from –120 to +40 mV, in 20-mV increments, were applied, and four pulses were averaged at each potential. Signals were filtered at 1 kHz and sampled at 2 kHz. To isolate the currents due to intramembrane charge movement from the capacitive transients, traces were fitted with a double exponential, and the slower component was corrected for any remaining leakage and integrated [30, 31]. Transport-associated currents were estimated by subtracting the traces in the absence of GABA from those in its presence for each experimental condition. Data analysis was performed using Clampfit 8.2 (Axon Instruments). All figures were prepared with Origin 5.0 (Microcal Software Inc., Northampton, MA, USA).

Cell culture and transfection

tsA201 cells were grown in Dulbecco's Modified Eagle Medium (DMEM) (Sigma-Aldrich, Italy) supplemented with 10% heat-inactivated foetal calf serum, 2 mM glutamine, 100 U/ml penicillin, 100 μg/ml streptomycin and were kept in a 5% CO_2 humidified atmosphere at 37 °C. Cells were plated in 35-mm dishes (1.4×10^5 cells per dish) and transfected with 1 μg of total DNA per dish using Lipofectamine 2000 (Invitrogen, Italy). In single-transfection experiments 400 ng of plasmid were used. In cotransfection experiments the different constructs were always used in a ratio of 1:1, respectively 400 ng each. An empty vector (pcDNA3.1, Invitrogen, Italy) was used to normalize the total amount of plasmid transfected. Cells were re-plated on round glass coverslips 24 h after the transfection and used 24 h after the re-plating procedure.

Fluorescent microscopy and image acquisition

tsA201 cells were observed 48 h after transfection. Fluorescence images were acquired with a Retiga 2000R cooled CCD camera (QImaging, Burnaby, BC, Canada) mounted on a Zeiss Axiovert IM35 inverted microscope, and through a Zeiss Fluar 40x oil immersion objective. Excitation was obtained by a 150 W Xenon arc lamp coupled to a filter wheel (CAIRN Research Ltd., Faversham, Kent, UK) delivering the light to the microscope through a light guide. Excitation filters were 430/25 nm for ECFP and 500/20 for EYFP; a neutral density filter (ND 0.2, transmittance approx. 63%) was used on the 500-nm excitation optic corridor. A double dichroic filter (86002 BS) was placed on the excitation light path to reflect both excitation wavelengths and pass both emissions. Emitted fluorescence reached an optosplit image splitter (CAIRN Research) fitted with a 495DCLP beam splitter, and two emission filters at 470/30 and 535/30 nm, for ECFP and EYFP, respectively. With this configuration donor, acceptor and FRET images could be obtained by changing only the excitation filters. For each excitation wavelength, the image splitter allowed capture of the two images (through the 470 nm and 535 nm emission filters) in the same frame on the CCD chip. In order to minimize photobleaching effects, an electronics-driven shutter was interposed between the excitation filters and the dichroic mirror, so that the cells were only excited for the time necessary to acquire the image. In these conditions, significant photobleaching of YFP occurred only after long-lasting exposures (>30 min). Images of the same set were acquired in identical conditions. All filters were from Chroma Technology Corporation, Rockingham, VT, USA.

Image analysis and FRET calculation

Images were analyzed with Image Pro Plus software (Media Cybernetics, Inc., Silver Spring, MD, USA). N_{FRET} images were constructed with the three filter set method, and following the analytical procedure introduced by [32]: images were subtracted by their relative background (obtained acquiring imaging in an area of the sample without cells, with the respective excitation configuration and CCD integration time); independent thresholding on the images was necessary to avoid image processing artefacts; donor and acceptor fluorescence bleed-through were calculated from cells transfected with rGAT1-ECFP and rGAT1-EYFP alone, according to [33], and subtracted from the FRET image, obtaining

the net FRET (*nF*) image; *nF* normalization was then performed by dividing the *nF* image by the square root of the donor acceptor product [32], see eq. (1).

$$N_{FRET} = \frac{I_{FRET} - I_{YFP} \times a - I_{CFP} \text{ x } b}{\sqrt{I_{YFP} \times I_{CFP}}} \quad (1)$$

where N_{FRET} is the normalized FRET value, and I_{FRET}, I_{YFP} and I_{CFP} are the intensities in each area of interest detected using FRET, EYFP and ECFP filter sets respectively. The constants $a = I_{FRET}/I_{YFP}$ and $b=I_{FRET}/I_{CFP}$ represent correction coefficients to account, respectively, for rGAT1-ECFP and rGAT1-EYFP bleed-through, under the FRET filter combination, calculated when only the donor (*b*) or the acceptor (a) were present. Data are presented as mean ± S.E. Experimental setup and analysis procedures have been optimized using a CFP-YFP tandem (generous gift of Dr. H. H. Sitte) which was constructed as a positive control for FRET imaging [21]. Cotransfection of ECFP and EYFP was used as negative control. ECFP and EYFP bleed-through coefficients were calculated in cells transfected only with ECFP and EYFP, respectively. All the calculations have been performed on floating point images.

Solutions

In electrophysiological experiments, the external control solution had the following composition (in mM): NaCl, 98; $MgCl_2$, 1; $CaCl_2$, 1.8; Hepes, 5 at pH 7.6. Equimolar NMDG (N-methyl-D-glutamine) or TMACl (tetramethylammonium chloride) were used as substitutes in Na^+-free solutions. The pH was adjusted with HCl, NaOH or TMAOH (tetramethylammonium hydroxide). GABA was added at the indicated micromolar concentrations to the appropriate solutions. Experiments were done at room temperature (20–24 °C). The specific rGAT1 blocker, SKF89976A (Tocris), was dissolved in sterile water and used at a final concentration of 30 μM.

In fluorescence experiments the extracellular control solution contained (in mM); 135 NaCl, 4 KCl, 1 $MgCl_2$, 2 $CaCl_2$, 6 glucose and 10 HEPES-NaOH at pH 7.35.

Results

Electrophysiological properties

Substitution of tyrosine 140 with tryptophan in rGAT1 was reported to result in a transporter defective in GABA and SKF89976A binding, but still able to interact with Na^+ to generate a voltage-dependent intramembrane charge movement [29]. This behaviour was confirmed in our electrophysiological experiments, summarized in figure 1. In control solution, containing 98 mM Na^+, the Y140W isoform exhibited transient currents only slightly different from the wild type. Besides a generally smaller level of expression (judged from the smaller amount of maximal charge movement, about 70% of the wild type in fig. 1C), the voltage dependences of the steady-state charge movement and of the equilibration rate constant were rather similar in the two isoforms. Only the decay rate of the transient current was significantly faster in the mutant. As shown in column B of figure 1, however, no changes in the current records were induced in Y140W by the addition of 300 μM GABA, a concentration that elicits maximal transport-associated currents in the wild type (column A). Na^+ ions do appear to be essential for the generation of the voltage-dependent charge movement, as substitution of these ions with NMDG or TMA removed the transient currents both in the wild type and in the mutant. Finally, Y140W was defective in SKF89976A binding: while addition of 30 μM of this blocker completely eliminated the transient currents in the wild type, the same treatment was completely ineffective in the mutant.

The amount of charge displaced to the inner transporter position (Q_{in}) in the wild type was compared in figure 1C (squares) with that of the mutant, estimated from the traces in the presence of Na^+ only (circles), or after addition of 300 μM GABA (triangles). Clearly no differences can be seen between these two last conditions. Fitting the data with a Boltzmann equation gives a half-charge voltage $V_{½}$ = –48.2 ± 2.2 mV and slope = 22.0 ± 0.5 mV for the wild type (n = 6), and $V_{½}$ = –32.8 ± 3.0 mV and slope = 20.8 ± 0.5 mV for Y140W (n = 5). The same negative shift was evident in the voltage-dependence of the equilibration rate of charge movement, plotted in figure 1D. Here again this parameter was estimated in the absence (circles) or presence (triangles) of 300 μM GABA, with identical results. Clearly, this process was significantly faster in the mutant compared with the wild type.

Finally, panel E of figure 1, shows that the transport-associated current measured in the wild type as the difference between the traces in the presence of 300 μM GABA and those in its absence, was well approximated by the product of the amount of charge displaced in the inner transporter position (Q_{in}) and the rate of charge equilibration at each potential [34, 35]. Clearly, this did not occur for the Y140W mutant, which cannot support transport.

Y140W may, therefore, be an appropriate tool to investigate the formation of functional oligomers. Its expression on the surface membrane may in fact be easily seen through electrophysiological methods; its behaviour may be separated from that of the wild type, taking advantage of insensitivity to SKF89976A block.

Coexpression experiments

We have then coinjected the cRNAs coding for wild type and Y140W in oocytes in equal amounts. Typical results from an oocyte expressing the two isoforms are shown

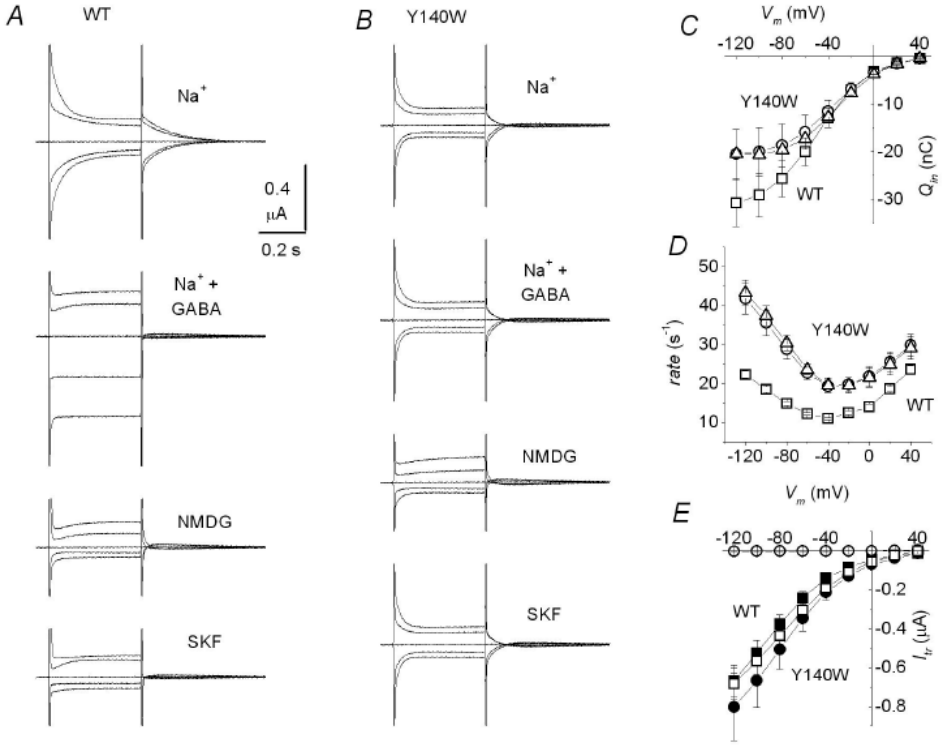

Figure 1. Electrophysiological characteristics of Y140W. (*A* and *B*) Membrane currents in response to 400 ms voltage pulses (range –120 to +40 mV from holding potential V_h = –40 mV) in two representative oocytes expressing wild-type (*A*) or Y140W (*B*) GAT1, in the indicated conditions. (*C*) Q vs V relationships obtained integrating the transient currents (average ± SE from six and five oocytes, respectively, from two batches) for wild-type (squares) and Y140W (circles, from traces in Na^+; triangles, from traces in the presence of GABA). (*D*) Equilibration rates from single exponential fitting of the transients (same oocytes and symbols as in *C*). (*E*) Transport-associated currents in the presence of 300 µM GABA from the same oocytes; open squares represent the measured average current in the wild-type, while the filled squares represent the Q_{in} x rate product using the corresponding values in panels *C* and *D*. No transport-associated current was detected in the Y140W mutant (open circles), although the Q_{in} x rate product predicts a current larger than in the wild-type (filled circles).

in column A of figure 2. Qualitatively, the current traces appeared to contain contributions from both isoforms: addition of GABA caused a conspicuous increase in steady-state levels, without, however, completely abolishing the transient phases. These disappeared when Na^+ was replaced by NMDG, but again SKF8997A was only partially effective in eliminating this kind of current.

Analysis of the transient currents from the coinjected oocytes was performed, trying to separate the GABA- and SKF89976A-resistant component from the sensitive component. To this end only the 'off' transients were used for integration, as these are less contaminated by time- and voltage-dependent transmembrane currents than the 'on' transients. To evaluate the SKF89976A-sensitive component, traces in the presence of 30 µM SKF89976A were subtracted from traces in Na^+, and the resulting "off" transients were then integrated; these data are shown as squares in figure 2B. The SKF89976A-resistant component was determined from traces in the presence of the blocker (fig. 2B, circles). Finally, integration of "off" transients remaining in the presence of 300 µM GABA was also performed (triangles in fig. 2B). Similarly to the observation in oocytes expressing Y140W only, the intramembrane charge movement resistant to SKF89976A was identical to that resistant to GABA, both in amplitude and in voltage dependence. Fitting of the sigmoidal curves with a Boltzmann function gives the following parameters: $V_{½}$ = –49.8 ± 2.9 mV and slope = 25.7 ± 1.0 mV for the SKF89976A-sensitive component (n = 12), and $V_{½}$ = –39.8 ± 1.9 mV and slope = 18.7 ± 0.7 mV for Y140W (n=12); these values were not significantly different from those determined in figure 1 from oocytes separately expressing the two isoforms (Student's *t* test; $p > 0.05$). The same separation procedure was used to estimate the rates of charge equilibration. In this case, however, the "on" transients must be used in order to obtain the voltage dependence of this parameter. The results are plotted in figure 2C, showing again that the SKF89976A- and GABA-resistant transients had faster rates (circles and triangles) compared with the sensitive component (squares). The absolute values of the rates of the components compare favourably with those of figure 1D, with the exception of those determined from the traces under GABA stimulation (probably contaminated by transmembrane currents). As a further check, the product of the rate and Q_{in} curves relative to the GABA- and SKF89976A-sensitive component is plotted in figure 2D, together with the transport-associated current determined experimentally. As in figure 1E for the wild type, the two sets of data match closely.

These observations suggest that in the 1:1 coinjection experiment both the wild-type and Y140W forms were expressed on the oocyte membrane. The two isoforms did not appear to functionally interact as, (i) the addition

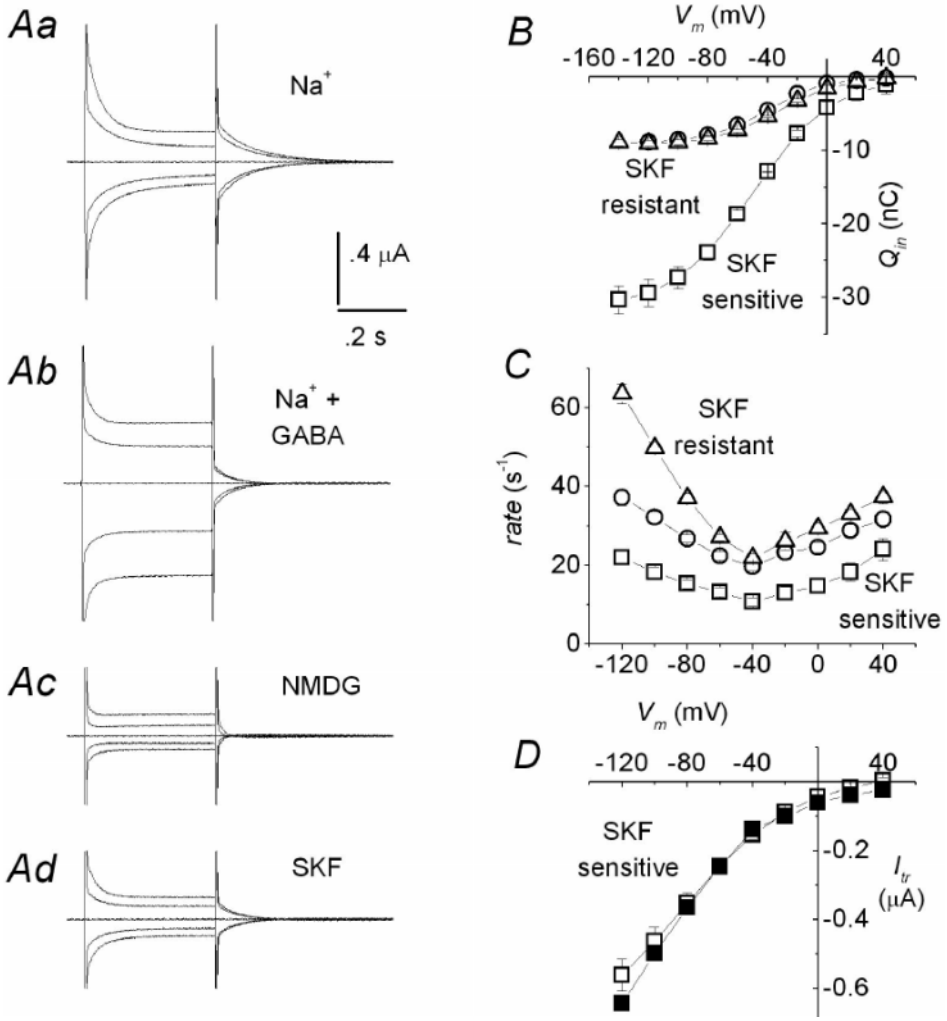

Figure 2. Coinjection of wild-type and Y140W GAT1. (*A*) Typical current traces recorded from an oocyte injected with equal amounts of wild-type and Y140W cRNA in response to 400 ms long voltage steps in the range –120 to +40 mV from V_h = –40 mV. In presence of 300 μM GABA a significant transport-associated current develops, although reduced transient currents are still present; these are abolished when Na^+ is replaced by NMDG. Addition of 30 μM SKF89976A again reveals the persistence of a component of the transient current resistant to the blocker. (*B*) separation of charge movement components: squares represent the blocker-sensitive component (*Aa–Ad*); circles represent the SKF89976A-resistant component (*Ad*), while triangles represent the GABA-resistant component (*Ab*). (*C*) Charge equilibration rates of the different components (same symbols as in *B*); the discrepancy between circles and triangles in the negative region is probably due to contamination of transmembrane ionic currents in the GABA-stimulated traces. (*D*) Transport-associated currents in the presence of 300 μM GABA from the same oocytes; open squares represent the measured average current (as in *Ab*), while the filled squares represent the Q_{in} x rate product using the values of the SKF89976A-sensitive component in panels *B* and *C*. Data are averages ± SE from 12 oocytes from three batches0.

of GABA, while producing a significant transport-associated current, did not completely abolish the transient current; (ii) the transient current remaining in presence of GABA coincided with the SKF89976A-resistant component; (iii) the voltage dependence of this component was indistinguishable from that observed in oocytes expressing the Y140W form alone; (iv) the SKF89976A-sensitive component had properties identical to those observed in oocytes expressing the wild-type form alone and, finally, (v) this component satisfied the condition that the product of the amount of charge displaced to the inner position by the equilibration rate in zero GABA gives the amplitude of the transport-associated current in presence of saturating GABA.

FRET analysis

These five observations indicated an absence of functional interaction between the wild-type and mutated forms of the transporter. However, the question whether rGAT1 operates as a functional oligomer needed a further control. In fact, although unlikely, considering the location of the Y140W mutation relative to the regions believed important for oligomerization, oligomers may occur only among identical subunits, so that wild-type subunits may oligomerize only with other wild-type subunits, and mutated subunits only with other mutated subunits. In order to check that mixed oligomers between wild-type and Y140W subunits may indeed form, we used a FRET approach.

Independent transfection of tsA201 cells with WT or Y140W rGAT1 fused at the COOH termini with ECFP or EYFP gave rise to fluorescence signals mainly localized at the plasma membrane level (not shown), with faint cytoplasmic fluorescence frequently associated with intracellular spots, confirming that the mutant was correctly localized to the plasma membrane in this cell

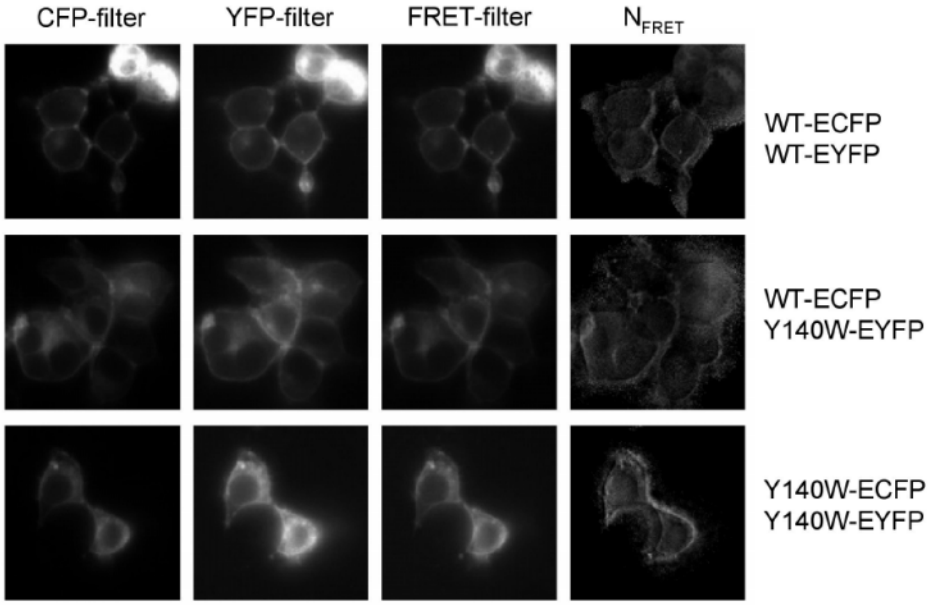

Figure 3. Fluorescence and N_{FRET} images from tsA201 cells transfected with the indicated combinations of vectors. Images were acquired through CFP-filter (ex. 430 nm, em. 470), YFP-filter (ex. 500 nm, em. 535 nm) and FRET-filter (ex. 430 nm, em. 535 nm) as indicated. N_{FRET} images were calculated as described in 'Materials and methods'. In all three cases a comparable degree of interaction is detected, suggesting that the Y140W mutation does not interfere with membrane localization and homo- or heterooligomer formation.

Table 1. N_{FRET} values derived from images calculated as explained in 'Materials and methods' for the indicated cotransfections

Cotransfection	Number of cells	N_{FRET} values
ECFP + EYFP	12	0.02 ± 0.01
WT-ECFP + WT-EYFP	12	0.43 ± 0.02 *
WT-ECFP + Y140W-EYFP	12	0.36 ± 0.01 *
Y140W-ECFP + Y140W-EYFP	12	0.50 ± 0.04 *

* Significantly different versus negative control (Student's *t*-test, $p < 0.01$).

line. These constructs proved to be functional in transfected tsA201 cells tested electrophysiologically using the whole-cell patch-clamp technique [our unpublished observations], confirming previous results [22, 36] showing that GAT1 is functional in a wild-type fashion when GFPs were attached either at the N-terminus or at the C-terminus. Three combinations of vectors were used for cotransfections: rGAT1-WT-ECFP/rGAT1-WT-EYFP, rGAT1-WT-ECFP/rGAT1-Y140W-EYFP and rGAT1-Y140W-ECFP/ rGAT1-Y140W-EYFP. The membrane distribution of tagged rGAT1 can be evaluated by looking at figure 3 (CFP and YFP filters). Images were acquired, from left to right, through the CFP-filter set (ex. 430 nm, em. 470 nm), the YFP-filter set (ex. 500 nm, em. 535 nm) and the FRET-filter set (ex. 430 nm, em. 535 nm).

The amount of fluorescence resonance was estimated as explained in 'methods', using eq. (1). N_{FRET} images of all the combinations used are shown in the last column of figure 3. In all three cases a FRET signal was clearly visible in zones coincident with the plasma membrane. A more diffuse cytoplasmic FRET signal was also present, confirming that the interaction also occurs at this level [37]. Table 1 shows the N_{FRET} values from the three combinations and for the negative control (cotransfection of ECFP and EYFP): the highly significant difference between constructs and negative control, and the fact that these values are comparable with those reported in the literature [32, 33], indicate that energy transfer occurs for all three cotransfections. We may then conclude that the Y140W mutation did not prevent formation of oligomers either with other mutant subunits or with WT subunits.

Discussion

The peculiar electrophysiological characteristics of the Y140W mutant of rGAT1 appear well suited to investigate the formation of functional oligomers. The persistence of the voltage-dependent transient currents demonstrates that Y140W is correctly inserted into the plasma membrane, while the inability to generate GABA-associated currents and the lack of SKF89976A effect make it easily distinguishable from the wild-type form. We have shown that the electrophysiological behaviour of oocytes coexpressing the wild-type and mutant transporters is perfectly consistent with independent functioning of the two forms. In particular, addition of saturating amounts of GABA, while eliciting transport-associated currents, does not completely abolish voltage-dependent transient currents. This remaining component is substantially identical, in terms of the amount of intramembrane charge movement and kinetic properties, to that remaining after

application of 30 μM SKF89976A (fig. 2). Subtraction of this GABA- and SKF89976A-resistant component from the total charge movement displayed by coinjected oocytes leaves a charge movement component whose characteristics match up well with those of the wild-type. Furthermore, for this component the product of the amount of charge displaced in the inner position times the charge equilibration rate (Q_{in} x r) corresponds well to the amplitude of the transport current in presence of saturating GABA. This feature was previously described to be an important property of wild-type rGAT1 functioning [34].

These results show that while both wild-type and mutant forms are present in the oocyte membrane, their electrophysiological behaviour and their ability to interact with GABA and with SKF89976A are preserved and remain independent.

While clearly pointing to independent behaviour of the two isoforms, the above results cannot exclude that only homooligomers may form; that is, wild type may oligomerize only with other wild-type subunits, and Y140W only with other Y140W subunits. Furthermore, Y140W may not form oligomeric structures at all. Although the regions believed to be important for oligomerization do not include transmembrane domain 3, where tyrosine 140 is located, the formation of homooligomers Y140W-Y140W, and heterooligomers Y140W-wild type was investigated using FRET.

Our results using ECFP- and EYFP-fused transporters in tsA201 cells showed that no differences in the amount of FRET could be observed comparing wild-type/wild-type, Y140W/Y140W or wild-type/Y140W pairs. In all cases the observed FRET signal is well localized to the cell membrane, and its level may be compared with those reported in the literature [21].

Besides confirming the membrane localization of Y140W, these data suggest that Y140W is able to form both homooligomers and heterooligomers with the wild-type form.

Our results thus indicate that although structural oligomerization of rGAT1 occurs, the single subunits operate individually. Oligomerization in rGAT1 does not appear to be directly involved in the transport mechanism, although its importance for the correct targeting of transporters to the membrane, with possible implications for its regulation [22], is supported by our data (fig. 3). These data show a diffused cytoplasmic FRET in all the cotransfections, suggesting a possible protein–protein interaction in the endoplasmic reticulum and/or in the Golgi, where the cotransporters are synthesized and processed. Furthermore, the atomic structure of $LeuT_{Aa}$ [8] shows a dimer in which each subunit separately interacts with two Na^+ ions and a leucine molecule, suggesting independent behaviour of each subunit. A similar dimeric structure was also recently proposed by Seidel and coworkers [26] for the human 5-HT transporter hSERT, with the additional possibility that the two subunits may operate in opposition, generating a countertransport system. This peculiar behaviour appeared to occur even in heterodimers formed by SERT and GAT [26]. Unfortunately, this kind of dependence between subunits cannot be tested in our electrophysiological experiments, which are only able to detect the operation of transporters in the outward-facing conformation. Further coupled influx and efflux measurements from cells coexpressing wild type and mutant transporters may possibly provide new information on this interesting new model.

Our conclusion about subunit independence was reached for other cotransporters as well [27, 28, 38, 39], and may mark an important difference between ionic channels and transporters. Similarly to transporters, most ionic channels appear to be formed by oligomers, or by repetitions of similar domains. In ionic channels, however, the functional role of oligomerization is of fundamental importance: point mutations in a single monomer of the tetrameric K^+ channel may alter toxin sensitivity [40]; the ionic selectivity of the voltage-dependent Na^+ channels may be changed by mutations in a single repeat of the four that contributes to the overall structure [41]. In contrast, transporters, although forming structural oligomers, often appear to function as individual monomers.

It may be appropriate to recall an interesting consideration by Kilic and Rudnick [12] stated in a paper in which they actually proposed functional interaction between subunits of the serotonin transporter: '*Small ions present a symmetrical surface to any protein with which they interact whereas carriers for more complex molecules must recognize an asymmetric substrate and in some cases discriminate between stereoisomers. An asymmetric binding site formed from many different TM domains would be more suited to binding complex substrates than a symmetrical binding site formed from identical TM domains.*'

We find this consideration quite convincing, and perhaps a good reason not to expect functional oligomerization as a general rule in transporter operation.

Acknowledgements. This work was supported by grants from the Italian Ministry of Research and University (FIRB program project No. RBAU01FKW2) and by a grant from the Fondazione CARIPLO to A. Peres. We are grateful to Prof. Riccardo Fesce for stimulating discussions.

1 Haugeto Ø., Ullesvang K., Levy L. M., Chaudhry F. A., Honoré T., Nielsen M. et al. (1996) Brain glutamate transporter proteins form homomultimers. J. Biol. Chem. **271:** 27715–27722

2 Gendreau S., Voswinkel S., Torres-Salazar D., Lang N., Heidtmann H., Detro-Dassen S. et al. (2004) A trimeric quaternary structure is conserved in bacterial and human glutamate transporters. J. Biol. Chem. **279:** 39505–39512

3 Yernool D., Boudker O., Jin Y. and Gouaux E. (2004) Structure of a glutamate transporter homologue from *Pyrococcus horikoshii*. Nature **431:** 811–818

4 Eskandari S., Kreman M., Kavanaugh M. P., Wright E. M. and Zampighi G. A. (2000) Pentameric assembly of a neuronal glutamate transporter. Proc. Natl. Acad. Sci. USA **97:** 8641–8646

5 Grunewald M., Bendahan A. and Kanner B. I. (1998) Biotynilation of single cysteine mutants of the glutamate transporter GLT-1 from rat brain reveals its unusual topology. Neuron **21:** 623–632

6 Sitte H.H. and Freissmuth M. (2003) Oligomer formation by Na^+-C^--coupled neurotransmitter transporters. Eur. J. Pharmacol. **479:** 229–236

7 Masson J., Sagné C., Hamon M. and El Mestikawy S. (1999) Neurotransmitter transporters in the central nervous system. Pharmac. Rev. **51:** 439–464

8 Yamashita A., Singh S. K., Kawate T. and Gouaux E. (2005) Crystal structure of a bacterial homologue of Na^+/Cl^--dependent neurotransmitter transporters. Nature **437:** 215–223

9 Horiuchi M., Nicke A., Gomeza J., Ashrafi A., Schmalzing G. and Betz H. (2003) Surface-localized glycine transporters 1 and 2 function as monomeric proteins in Xenopus oocytes. Proc. Natl. Acad. Sci. USA **98:** 1448–1453

10 Kokabas A. M., Rudnick G. and Kilic F. (2003) Functional consequences of homo- but non hetero-oligomerization between transporters for the biogenic amine neurotransmitters. J. Neurochem. **85:** 1513–1520

11 Jess U., Betz H. and Schloss P. (1996) The membrane-bound rat serotonin transporter, SERT1, is an oligomeric protein. FEBS Lett. **394:** 44–46

12 Kilic F. and Rudnick G. (2000) Oligomerization of serotonin transporter and its functional consequences. Proc. Natl. Acad. Sci. USA **97:** 3106–3111

13 Torres G. E., Carneiro A., Seamans K., Fiorentini C., Sweeney A., Yao W. D. et al. (2003) Oligomerization and trafficking of the human dopamine transporter. Mutational analysis identifies critical domains important for the functional expression of the transporter. J. Biol. Chem. **278:** 2731–2739

14 Hastrup H., Karlin A. and Javitch J. A. (2001) Symmetrical dimer of the human dopamine transporter revealed by cross-linking Cys-306 at the extracellular end of the sixth transmembrane segment. Proc. Natl. Acad. Sci. USA **98:** 10055–10060

15 Hastrup H., Sen N. and Javitch J. A. (2003) The human dopamine transporter forms a tetramer in the plasma membrane. J. Biol. Chem. **278:** 45045–45048

16 Norgaard-Nielsen K., Norregaard L., Hastrup H., Javitch J. A. and Gether U. (2002) Zn^{2+} site engineering at the oligomeric interface of the dopamine transporter. FEBS Lett. **524:** 87–91

17 Remmers A. E. (1998) Detection and quantitation of heterotrimeric G proteins by fluorescence resonance energy transfer. Anal. Biochem. **257:** 89–94

18 Angers S., Salahpour A., Joly E., Hilairet S., Chelsky D., Dennis M. et al. (2000) Detection of β_2-adrenergic receptor dimerization in living cells using bioluminescence resonance energy transfer (BRET). Proc. Natl. Acad. Sci. USA **97:** 3684–3689

19 Riven I., Kalmanzon E., Segev L. and Reuveny E. (2003) Conformational rearrangements associated with the gating of a G protein-coupled potassium channel revealed by FRET microscopy. Neuron **38:** 225–235

20 Sorkina T., Doolen S., Galperin E., Zahniser N. R. and Sorkin A. (2003) Oligomerization of dopamine transporters visualized in living cells by fluorescence resonance energy transfer microscopy. J. Biol. Chem. **278:** 28274–28283

21 Schmid J. A., Scholze P., Kudlacek O., Freissmuth M., Singer E. A. and Sitte H. H. (2001) Oligomerization of the human serotonin transporter and of the rat GABA transporter 1 visualized by fluorescence resonance energy transfer microscopy in living cells. J. Biol. Chem. **276:** 3805–3810

22 Scholze P., Freissmuth M. and Sitte H. H. (2002) Mutations within an intramembrane leucine heptad repeat disrupt oligomer formation of the rat GABA transporter 1. J. Biol. Chem. **277:** 43682–43690

23 Korkhov V. M., Farhan H., Freissmuth M. and Sitte H. H. (2004) Oligomerization of the γ-aminobutyric acid transporter-1 is driven by an interplay of polar and hydrophobic interactions in transmembrane helix II. J. Biol. Chem. **279:** 55728–55736

24 Just H., Sitte H. ., Schmid J. A., Freissmuth M. and Kudlacek O. (2004) Identification of an additional interaction domain in transmembrane domains 11 and 12 that supports oligomer formation in the human serotonin transporter. J. Biol. Chem. **279:** 6650–6657

25 Kitayama S., Ikeda T., Mitsuhata C., Sato T., Morita K. and Dohi T. (1999) Dominant negative isoform of rat norepinephrine transporter produced by alternative RNA splicing. J. Biol. Chem. **274:** 10731–10736

26 Seidel S., Singer E. A., Just H., Farhan H., Scholze P., Kudlacek O. et al. (2005) Amphetamines take two to tango: an oligomer-based counter-transport model of neurotransmitter transport explores the amphetamine action. Mol. Pharmacol. **67:** 140–151

27 Koch H. P. and Larsson H. P. (2005) Small-scale molecular motions accomplish glutamate uptake in human glutamate transporters. J. Neurosci. **25:** 1730–1736

28 Grewer C., Balani P., Weidenfeller C., Bartusel T., Tao Z. and Rauen T. (2005) Individual subunits of the glutamate transporter EAAC1 homotrimer function independently of each other. Biochemistry **44:** 11913–11923

29 Bismuth Y., Kavanaugh M. P. and Kanner B. I. (1997) Tyrosine 140 of the γ-aminobutyric acid transporter GAT-1 plays a critical role in neurotransmitter recognition. J. Biol. Chem. **272:** 16096–16102

30 Hazama A., Loo D. D. F. and Wright E. M. (1997) Presteady-state currents of the rabbit Na^+/glucose cotransporter (SGLT1). J. Membr. Biol. **155:** 175–186

31 Forster I. C., Biber J. and Murer H. (2000) Proton-sensitive transitions of renal type II Na^+-coupled phosphate cotransporter kinetics. Biophys. J. **79:** 215–230

32 Xia Z. and Liu Y. (2001) Reliable and global measurement of fluorescence resonance energy transfer using fluorescence microscopes. Biophys. J. **81:** 2395–2402

33 Gordon G. W., Berry G., Liang X. H., Levine B. and Herman B. (1998) Quantitative fluorescence resonance energy transfer measurements using fluorescence microscopy. Biophys. J. **74:** 2702–2713

34 Fesce R., Giovannardi S., Binda F., Bossi E. and Peres A. (2002) The relation between charge movement and transport-associated currents in the GABA cotransporter rGAT1. J. Physiol. **545:** 739–750

35 Peres A., Giovannardi S., Bossi E. and Fesce R. (2004) Electrophysiological insights on the mechanism of ion-coupled cotransporters. NIPS **19:** 80–84

36 Chiu C.-S., Jensen K., Sokolova I., Wang D., Li M., Deshpande P. et al. (2002) Number, density and surface/cytoplasmic distribution of GABA transporters at presynaptic structures of knock-in mice carrying GABA transporter subtype 1-green fluorescent protein fusions. J. Neurosci. **22:** 10251–10266

37 Sitte H. H., Farhan H. and Javitch J. A. (2004) Sodium-dependent neurotransmitter transporters: oligomerization as a determinant of transporter function and trafficking. Mol. Interv. **4:** 38–47

38 Köhler K., Forster I. C., Lambert G., Biber J. and Murer H. (2000) The functional unit of the renal type IIa Na^+/P_i cotransporter is a monomer. J. Biol. Chem. **275:** 26113–26120

39 Veenhoff L. M., Heuberger E. H. M. L. and Poolman B. (2002) Quaternary structure and function of transport proteins. TIBS **27:** 242–249

40 MacKinnon R. (1991) Determination of the subunit stoichiometry of a voltage-activated potassium channel. Nature **350:** 232–235

41 Sather W. A., Yang J. and Tsien R. W. (1994) Structural basis of ion channel permeation and selectivity. Curr. Opin. Cell Biol. **4:** 313–323